Journal of Coastal Research	SI	95	1473–1479	Coconut Creek, Florida	2020

Hydrodynamics on a Rocky Shore under Moderate-energy Wave Conditions

Laura Lavaud[†], Marc Pezerat[†], Thibault Coulombier[†], Xavier Bertin[†], and Kévin Martins[†‡]

[†]UMR LIENSs
CNRS-La Rochelle Université
La Rochelle, France

[‡]UMR 5805 EPOC
CNRS-Université de Bordeaux
Pessac, France

www.cerf-jcr.org

www.JCRonline.org

ABSTRACT

Lavaud, L.; Pezerat M.; Coulombier, T.; Bertin, X., and Martins, K., 2020. Hydrodynamics on a rocky shore under moderate-energy wave conditions. *In:* Malvárez, G. and Navas, F. (eds.), *Global Coastal Issues of 2020*. *Journal of Coastal Research*, Special Issue No. 95, pp. 1473-1479. Coconut Creek (Florida), ISSN 0749-0208.

Wave hydrodynamics on rocky shore platforms can be different from that on sandy beaches, namely due to a higher bed roughness. This study investigates short and infragravity waves transformation on a A-type rocky shore platform under moderate-energy wave conditions. Seven pressure sensors and two current meters were deployed along a cross-shore transect topped by a steep sandy beach. Data analysis complemented with a 1D model of energy flux conservation for short and infragravity waves reveals that commonly used value for the bottom drag coefficient has to be multiplied by 20 to match the field observations. Incoming infragravity waves suffer a strong dissipation at low tide due to bottom friction, while a slight shoreward increase is observed at high tide. Further analysis shows that, at this tidal stage, infragravity waves are almost fully reflected.

ADDITIONAL INDEX WORDS: *Rocky shore platform, wave hydrodynamics, bed roughness, field measurement.*

INTRODUCTION

Shore platforms are gently sloping or sub-horizontal rock surfaces often located in the intertidal zone. Sunamura (1992) categorized shore platforms in two major morphological types: Type A platforms are gently sloping ($\tan\alpha \approx 0.01 - 0.05$) and can be found in environments with moderate to large tidal ranges (mean spring tidal range > 2 m); Type B platforms are characterized by a quasi-horizontal surface with a sharp seaward edge and usually develop in environments with small tidal ranges (mean spring tidal range < 2 m). Since both wave erosion and subaerial weathering were identified as processes driving rocky shore platform evolution, there has been a long-standing debate on which is the dominant mechanism. It is now recognized that shore platform development is controlled by a combined action of these processes, although their relative contributions are still unclear (Stephenson, Kirk, and Hemmingsen, 2019).

Investigating wave transformation processes on shore platforms is thus of key importance to better understand the role of waves in their development, while field observations are still rare in the literature (Naylor, Stephenson, and Trenhaile, 2010). Nonetheless, several studies were carried out over the last 20 years, improving knowledge about short and infragravity wave transformation on shore platforms (Beetham and Kench, 2011; Farrell *et al*., 2009; Marshall and Stephenson, 2011; Ogawa, 2013; Ogawa, Dickson, and Kench, 2011, 2015; Ogawa, Kench, and Dickson, 2012; Stephenson and Kirk, 2000). Morphological features of the platform (gradient, width and elevation) and hydrodynamic forcings (incident wave energy and tides) were shown to have a key control on short wave energy dissipation (Beetham and Kench, 2011; Marshall and Stephenson, 2011; Ogawa, Dickson, and Kench, 2011, 2015). Conversely, the latter studies reported a shoreward increase in infragravity wave height. While these studies were carried out in micro- to mesotidal environments, field measurements carried out under macrotidal regimes are still scarce (Brayne, 2016; Poate *et al*., 2018, 2019; Stephenson *et al*., 2018; Trenhaile and Kanyaya, 2007). Poate *et al*. (2018) investigated the role of bed roughness on wave transformation on A-type rocky platforms. They compared contributions of wave breaking and frictional effects to short wave dissipation and suggested that friction is significant in the shoaling zone for very rough and flat platform, under small wave conditions.

Combining new field measurements and numerical models are required to improve the understanding of wave processes on rocky platforms, in particular the effects of bed roughness on platform hydrodynamics. This paper investigates short and infragravity wave transformation on a macrotidal rocky platform and examines the potential effect of a higher bed roughness.

METHODS

Study Area

The studied shore platform is located at Matha, along the Western coast of the Oléron Island in the central part of the French Atlantic Coast (Figure 1). The continental shelf in the region is about 150 km-wide and the Oléron island is characterized by gently sloping shorefaces. The tidal regime is semi-diurnal and macrotidal, with a minimum tidal range during neap tides of ~1.10 m and a maximum of ~5.50 m during spring tides. Dodet *et al*. (2019) analysed wave regimes along the 30 m isobath line

DOI: 10.2112/SI95-284.1 received 31 March 2019; accepted in revision 13 February 2020.
*Corresponding author: laura.lavaud@univ-lr.fr

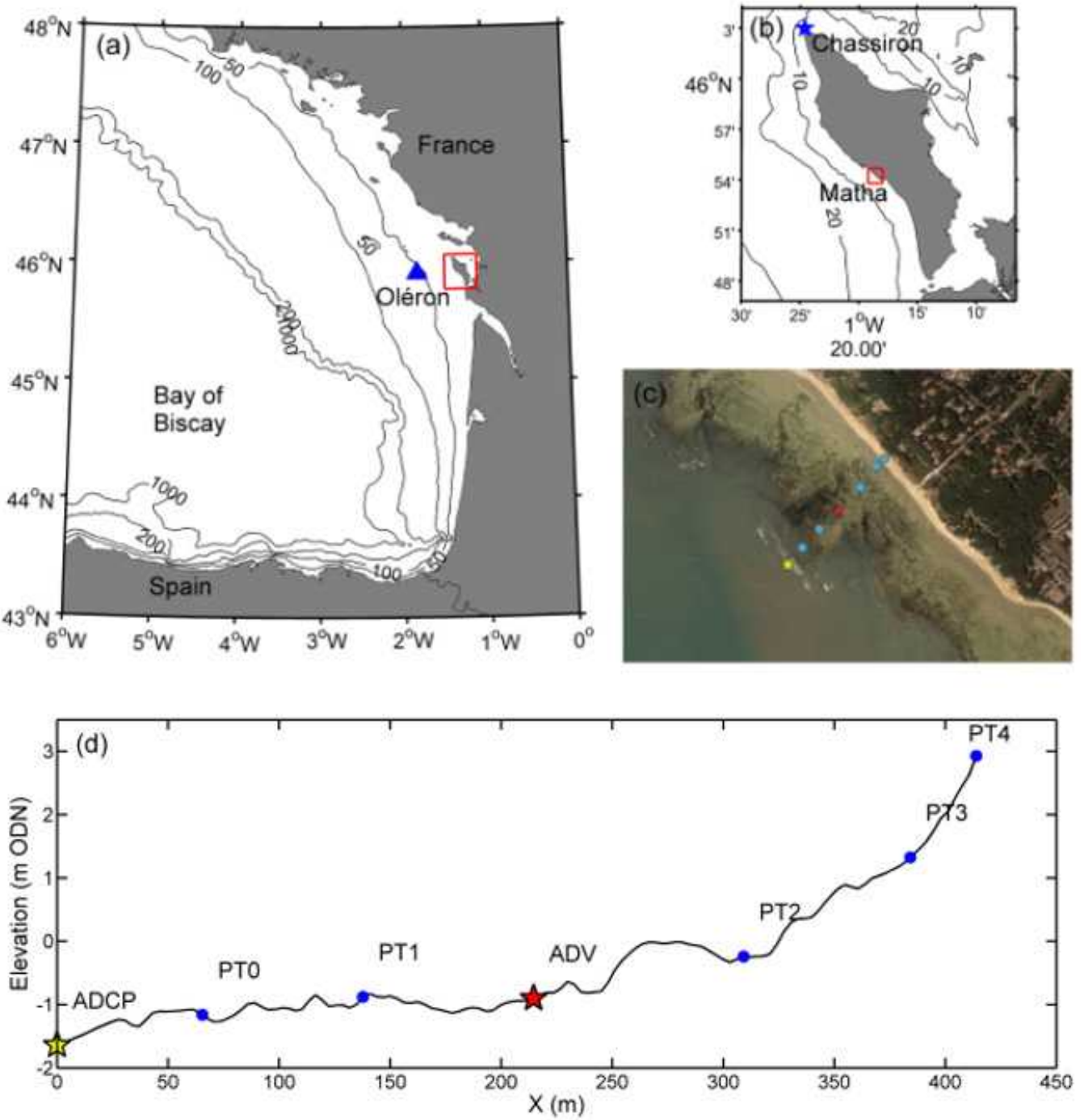

Figure 1. Location of the Oléron Island in the Bay of Biscay (red box) and Oléron wave buoy (blue triangle) (a). Location of the study area (red box) and the meteorological station (blue star) (b). Aerial image with location of the ADCP (yellow star), the ADV (red star) and the pressure sensors (PT) (blue points). Cross-shore profile of the field site (d).

of the metropolitan coasts of France and reported in the region yearly-averaged significant wave height of 1.60 m and yearly averages of mean wave period and wave direction of 5.9 s and 275° respectively.

The Matha shore platform is gently sloping ($\tan\alpha \approx 0.004$ and increases up to 0.02 at the top of the platform, from x = 300 m to x = 380 m, see Figure 1d), 400 m in length and backed by a sandy dune with a steep sandy beach at the platform-dune junction. The platform is a marl-limestone formation characterised by shallow steps and pools.

Field Campaign and Data Processing

A 1-day field campaign was performed in March 2019 on the Matha shore platform under spring tides with a 5.5 m tidal

range. Wave conditions were moderate, with a maximum offshore significant wave height of 1.4 m, recorded at the nearby Datawell Oléron buoy (Figure 1a). Five pressure sensors sampling at 2 Hz, an ADCP (head frequency 2 MHz) and an ADV (head frequency 6 MHz), both equipped with a pressure sensor, were deployed along a cross-shore transect in the intertidal zone. The deployment covered almost the full spring intertidal zone, which allowed to instrument both the shoaling and surf zones. The instruments were protected by steel tubes screwed to the bedrock with a spacing of approximately 75 m. Field data from PT4 could not be used since the sensor was emerged most of the time.

Bottom pressure measurements were first corrected for sea level atmospheric pressure measured at the nearby meteorological station of Chassiron (Figure 1b). Each data record was then analysed using consecutive bursts of 20 min, during which the sensor was continuously submerged. A Fast Fourier Transform with 5 Hanning-windowed segments overlapped by 50 % (10 degrees of freedom) was used to calculate the bottom pressure energy density spectra $E_p(f)$. $E_p(f)$ were then converted into elevation spectra $E(f)$ according to the linear wave theory. The significant wave height H_{m0} was computed as:

$$H_{m0} = 4\sqrt{m_0} \tag{1}$$

And

$$m_0 = \int_{f_{min}}^{f_{max}} E(f)\,df \tag{2}$$

where f_{max} = 0.4 Hz and f_{min} = 0.04 Hz for the gravity band, while frequencies lower than 0.04 Hz correspond to the infragravity band.

The low-pass filtered surface elevation η_{lf} was partitioned into incoming and outgoing infragravity wave (IGW) signals at the ADCP and the ADV, using the time-domain approach of Guza, Thornton, and Holman (1985):

$$\eta_{lf}^{\mp} = \frac{\eta_{lf} \mp \sqrt{h/g}\,u_{lf}}{2} \tag{3}$$

where u_{lf} is the low-pass filtered cross-shore velocity, h is the mean water depth and g is the gravitational acceleration. This separation was only performed for water depths larger than 1.0 m to guaranty that the sensors were always outside the swash zone. Incoming and outgoing significant IGW heights $H_{mo,ig,\mp}$ were then computed similarly as H_{m0} (Eq. 1).

Modelling Wave Transformation

The evolution of short and IGW heights along the cross-shore profile is investigated through the application of the wave height transformation model of Thornton and Guza (1983). A 1D model of energy flux conservation has already been applied to IGW (van Dongeren *et al.*, 2007). For straight and parallel depth contours, the energy flux balance is:

$$\frac{\partial EC_g}{\partial x} = -D_{break} - D_{bfric} \tag{4}$$

where $E = \frac{1}{8}\rho g H_{rms}^2$ is the energy density with ρ the density of seawater and H_{rms} the root-mean-square wave height. C_g is the wave group velocity, D_{break} is the wave breaking dissipation and D_{bfric} is the dissipation by bottom friction.

Dissipation by bottom friction is computed according to Thornton and Guza (1983):

$$D_{bfric} = \rho C_f \frac{1}{16\sqrt{\pi}}\left[\frac{2\pi H_{rms}}{T_p \sinh k_p h}\right]^3 \tag{5}$$

where C_f is the bottom drag coefficient, T_p and k_p are the peak wave period and the corresponding wave number respectively.

Dissipation by wave breaking is computed according to Thornton and Guza (1983):

$$D_{break} = \frac{3\sqrt{\pi}}{16}\rho g B^3 \frac{1}{T_p}\frac{H_{rms}^5}{\gamma^2 h^3}\left[1 - \frac{1}{\left(1+\left(H_{rms}/\gamma h\right)^2\right)^{5/2}}\right] \tag{6}$$

where B is a breaker coefficient of O(1) (Thornton and Guza, 1983) and γ is the breaker index corresponding to the maximum H_{rms} to water depth ratio in the inner surf zone. In this study, B is set to 1, the energy flux balance is therefore controlled by two adjustable parameters, γ and C_f. In IGW dissipation parametrisations (Eqs. 5-6), T_p is substituted by the mean wave period $T_{m02,ig}$, computed in the infragravity band.

Eq. 4 is solved using a simple finite difference scheme, taking observations from the seaward instrument (ADCP) as the boundary conditions (x = 0, see Figure 1d). The peak period T_p and the mean wave period $T_{m02,ig}$ are kept constant along the transect. The bathymetry of the transect originates from LIDAR data provided by the French National Geographic Institute (IGN) and the French Naval Hydrographic and Oceanographic Department (SHOM) through the Litto3D database. The profile is smoothed using a 10 m moving average filter.

RESULTS

In this section, predictions of Eq. 5 are compared to the field observations. For each burst, the model error is quantified by computing the Root Mean Square Error (RMSE) and the bias between the observed and modelled H_{m0} (Field data at the ADCP are not considered as they are used to force the model).

Wave Characteristics

Significant wave heights of short wave $H_{m0,sw}$ and total IGW $H_{m0,ig}$ during the field campaign are presented in Figure 2. Both $H_{m0,sw}$ and $H_{m0,ig}$ are tidally modulated with a peak of 1 m (resp. 0.19 m) at high tide and a minimum of about 0.18 m (resp. 0.12 m) at low tide.

Short Wave Transformation

The model errors are minimized by adjusting C_f oustide the surf zone. Simulations are performed with different values of C_f while γ is kept at the constant value of 0.42 (Thornton and Guza, 1983).

Figure 3 shows the comparison of observed and modelled $H_{m0,sw}$ at the first high tide for two values of C_f, 0.01, used for sandy beaches (Thornton and Guza, 1983) and 0.2. With C_f = 0.2, the model much better matches the observations with a RMSE divided by 5 and a bias almost cancelled out. The platform roughness enhances energy dissipation by friction, which results in a decrease of the wave height from 1.0 m by a water depth of ~ 4.50 m (x = 0 m) to 0.6 m at the beginning of the surf zone

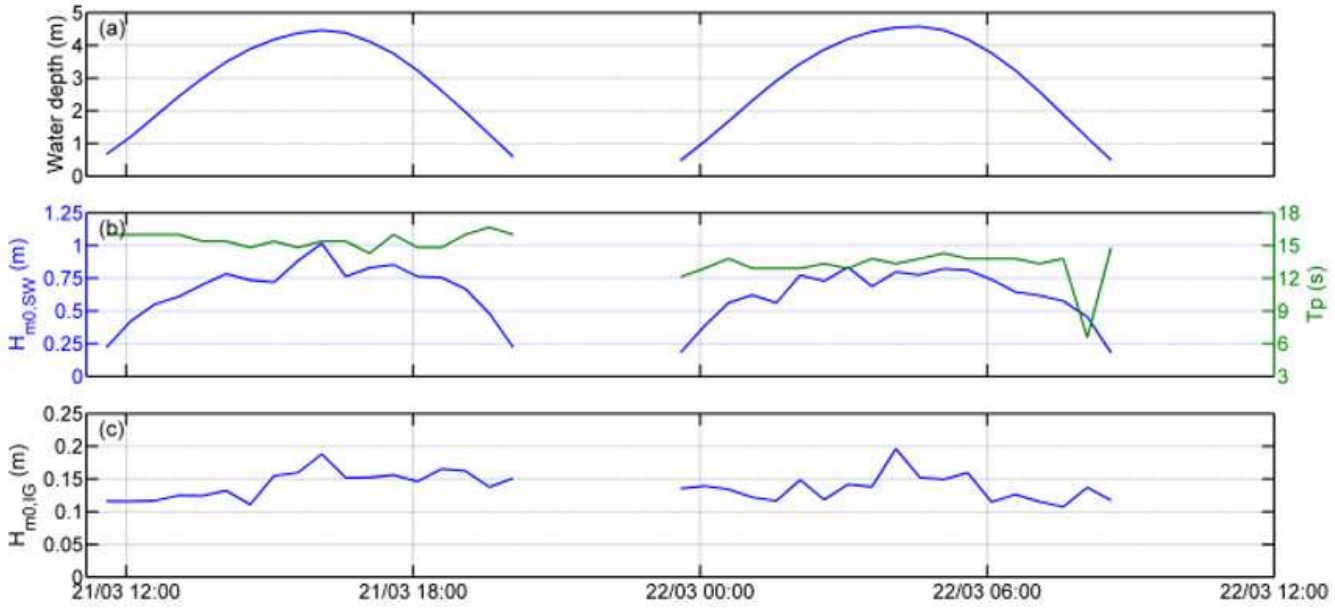

Figure 2. Water depth (a). Significant short wave height and peak period (b) and significant IGW height (c) at the ADCP.

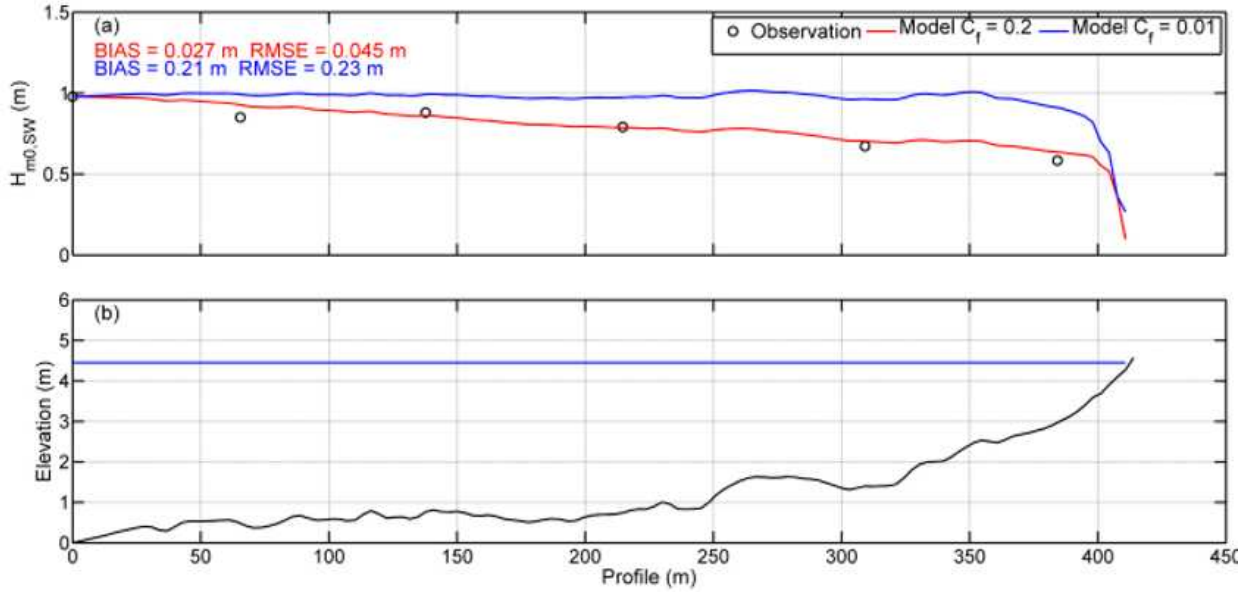

Figure 3. Observed against modelled significant short wave height with C_f = 0.2 (red line) and C_f = 0.01 (blue line) during the first high tide (a). Corresponding elevation along the transect (b).

(x = 380 m). Indeed, wave breaking occurs very close to the shoreline at high tide and pressure sensors are located seaward of the surf zone, where wave energy dissipation is dominated by bottom friction (Figure 3a). Data recorded up to x = 350 m provide therefore a reliable estimation of C_f .

Infragravity Wave Transformation

Infragravity wave transformation across the shore platform is firstly examined through the comparison of the observed $H_{m0,ig,+}$ at the ADV and the model (Figure 4).

At low tide, $H_{m0,ig,+}$ decreases (from 0.11 to 0.08 m) across the platform (Figure 4a) while at higher tidal levels, $H_{m0,ig,+}$ remains constant (not shown) or slightly increases (from 0.14 to 0.16 m) (Figure 4b). The comparison at low tide (Figure 4a) between the model without energy dissipation (conservative shoaling) and the observations at the ADV shows that the model overestimates $H_{m0,ig,+}$ (0.12 m against 0.08 m) while the model accounting for dissipation (D_{break} and D_{bfric}) reproduces well $H_{m0,ig,+}$, with a bottom drag coefficient C_f of 0.2. At high tide (Figure 4b), the comparison reveals that both models underestimate $H_{m0,ig,+}$

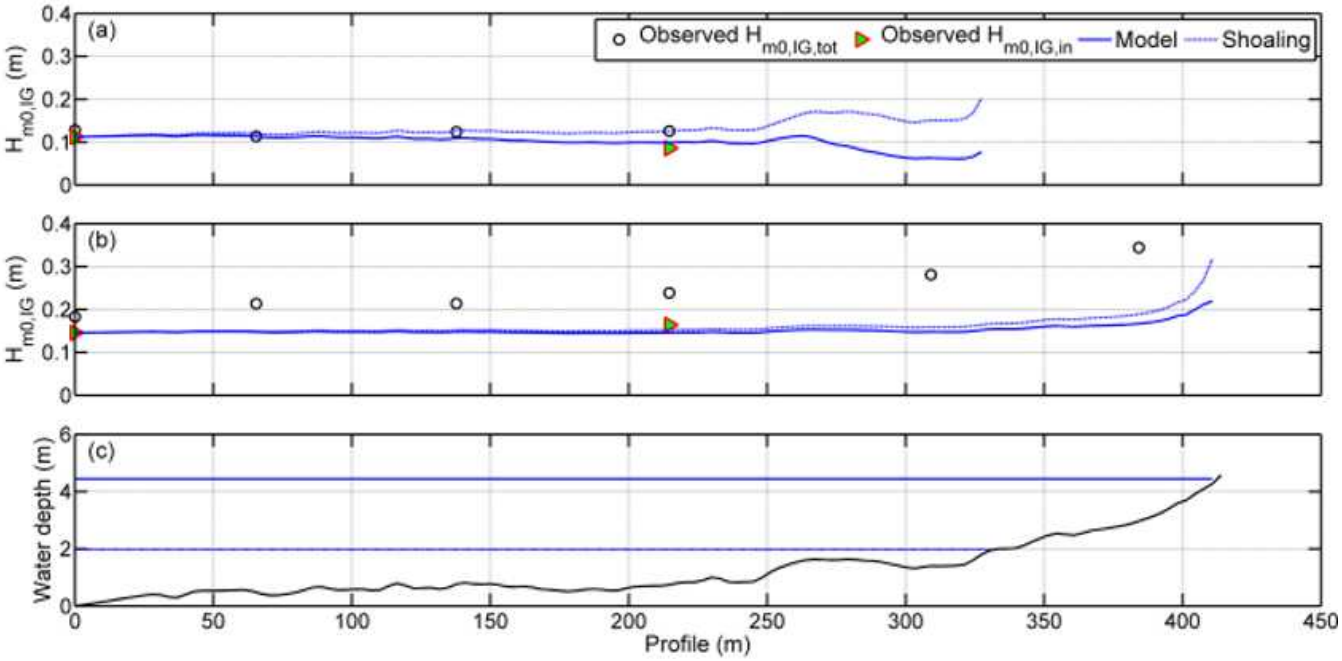

Figure 4. Observed total and incoming IGW heights against modelled incoming IGW height with dissipation accounted for (solid line), and conservative shoaling (dashed line) at low (a) and high tides (b). Elevation at low (dashed line) and high tides (solid line) (c).

(~0.14 m against 0.16 m at the ADV), the model without energy dissipation resulting in slightly better predictions. Overall, these results suggest that the IGW are dissipated by bottom friction across the platform at low tidal stages, which is well predicted. At higher tidal levels, this process is less significant due to increased water depth (cf Eq. 5) and balanced by another process responsible for the increase in $H_{m0,ig,+}$, which seems to be not accounted for by the model.

Figure 4 also reveals differences between observed $H_{m0,ig,+}$ and total $H_{m0,ig}$: while at low tide $H_{m0,ig}$ and $H_{m0,ig,+}$ profiles across the platform are similar (Figure 4a), $H_{m0,ig}$ is higher than $H_{m0,ig,+}$ at high tide (0.24 m against 0.16 m at the ADV) (Figure 4b), which suggests a tidal modulation of wave reflection.

DISCUSSION

The combination of data analysis and numerical modelling reveals firstly that short waves are dissipated across the platform through both frictional effects and wave breaking. The optimum bottom drag coefficient is found to be equal to 0.2, which is 20 times the value recommended for sandy beaches (0.01; Thornton and Guza, 1983) while being of the order of the values reported in the literature for coral reefs (0.16, 0.22 in Falter, Atkinson, and Merrifield (2004) and Lowe *et al*. (2005) respectively). Poate *et al*. (2018) investigated the effect of bed roughness on wave transformation across rocky platforms with the same model as in the present study. They reported scattered values of the bottom drag coefficient C_f calibrated at their roughest field sites (0.0005 and 0.34). An empirical estimation of C_f based on the platform roughness did not improve the results, which thus questioned the validity of the model for very rough platforms, suggesting that frictional dissipation in this case should be further parametrized with phase-resolving numerical models. Overall, their model results showed that frictional dissipation is significant at the roughest site (C_f = 0.34) while short wave dissipation across the other platforms is dominated by wave breaking. The results of the present study suggest that short wave dissipation by bottom friction highly controls the wave energy entering the surf zone under moderate energy conditions, which is demonstrated by the high value of C_f (0.2) required to well predict the short wave evolution across the platform.

As another important result, the incoming IGW height decreases at low tidal phases while increases across the shore platform at higher tidal stages. IGW can be generated by the bound long wave mechanism (Longuet-Higgins and Stewart, 1962) or the breakpoint forcing mechanism (Symonds, Huntley, and Bowen, 1982). In the first case, the incoming bound wave is theoretically out of phase with the short wave energy envelope. When propagating in shallower waters over a sloping bottom, the bound wave lags behind the wave groups (van Dongeren *et al*., 2007). This process allows additional energy transfer from short waves to the bound IGW compared to a simple conservative shoaling. A cross-correlation analysis is performed at the ADCP and the ADV between the short-wave envelope and the incoming IGW to examine if this can explain the shoreward increase in IGW height. A strong negative correlation (r = -0.6) is found between the two signals, suggesting that the incoming IGW is generated through the bound wave mechanism, and corresponds to a time lag of the order of 3 s for the whole tidal cycle, meaning that the IGW lags behind the wave group. This result is supported by the findings of Jager (2016) and Poate *et al*. (2019), who showed that IGW generation on A-type shore platforms is related to the bound long wave mechanism. Jager (2016) combined field data analysis on a macrotidal sloping shore platform and numerical modelling with the X-Beach modelling system and suggested that the evolution of IGW across the shore platform is tidally modulated. At high tide, IGW increase, mainly due to the bound long wave mechanism,

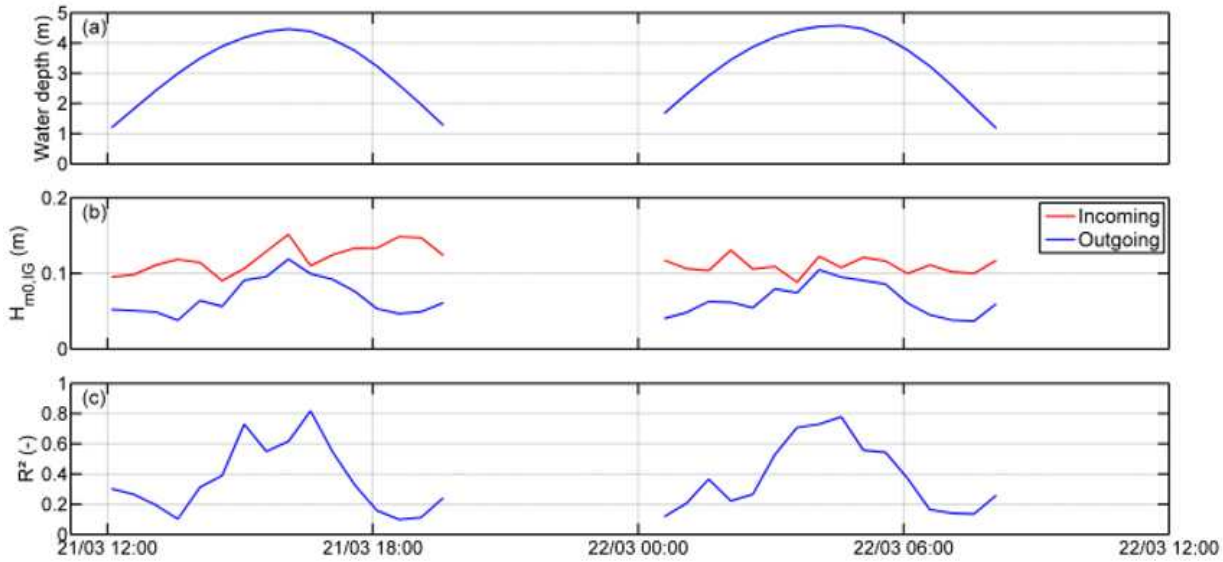

Figure 5. Water depth during the field campaign (a). Incoming and outgoing IGW height (b). Reflection coefficent R² (c).

while for mid-tidal phases, the growth rate is lower and the IGW height can even decrease due to a larger interaction with the platform roughness.

The differences between $H_{m0,ig,+}$ and the total IGW height $H_{m0,ig}$ at the two tidal phases (Figure 4) reveal a tidal modulation of wave reflection, this process being stronger at high tide when the water line corresponds to a steep-sloping beach. The reflection can be quantified by determining the IGW reflection coefficient, which can be related to the parameter β_H proposed by van Dongeren *et al*. (2007):

$$\beta_H = \frac{h_x T_{m02,ig}}{2\pi}\sqrt{\frac{g}{H_{m0,ig,+}}}$$

where h_x is the bottom slope. The authors carried out laboratory measurements and suggested that the IGW reflection is full for $\beta_H > 1.25$. β_H is computed at the shoreline at high and low tides where h_x is 1/20 and 1/250 respectively. While at high tide, β_H equals 3.1, suggesting a full reflection of the IGW, β_H equals 0.45 at low tide, implying a weaker reflection. The reflection is further analysed by computing the reflection coefficient R² at the ADCP, which corresponds to the ratio between the incoming and outgoing energy. The reflection process seems to be tidally modulated with reflection coefficient reaching 0.8 at high tides and decreases to less than 0.2 at low tides (Figure 5). These results are in line with the work of Jager (2016), who found that the reflection coefficient at the shoreline is stronger at high tide, during which the growth rate of incoming IGW is higher and the shoreline faces the steep-sloping cliff.

Considering that a full reflection occurs at high tide ($R^2 = 1$), the underestimation of modelled incoming energy pointed out at this tidal stage (Figure 4b) can be supported by computing the total IGW height $H_{m0,ig}$ at the most landward sensor. Modelled $H_{m0,ig,+} = 0.17$ m at this location and $H_{m0,ig} = \sqrt{2}.H_{m0,ig,+}$ with $R^2 = 1$, resulting in $H_{m0,ig} = 0.24$ m. This value is ~30 % lower than the observed $H_{m0,ig}$ (0.35 m), showing that the model underestimates $H_{m0,ig,+}$. These results suggest that the evolution of IGW across the platform can not be properly predicted using a simple energy flux conservation model but requires the use of surf-beat or phase-resolving models to account for energy transfer from short waves to the bound IGW.

CONCLUSIONS

Wave transformation across a A-type rocky shore platform is investigated through the analysis of field measurements complemented with a 1D model of energy flux conservation. To match the observations, a bottom drag coefficient 20 times the typical value reported in the literature for sandy beaches is required. Further analysis suggests that IGW are dissipated by bottom friction at low tide. At higher tidal stages, they increase, due to energy transfer from short waves to the bound IGW and less frictional dissipation, while suffering a strong reflection on the steep-sloping beach that tops the platform. A new field campaign under more energetic wave conditions will be carried out during winter of 2019/2020 to verify these findings and conduct further analysis, such as the effect of a high bed roughness on the wave setup. This study will combine field observations with the 3D modelling SCHISM (Zhang *et al*., 2016), representing wave-current interactions using a vortex force formalism as described in Guérin *et al*. (2018). IGW evolution will be investigated with SCHISM in surf-beat mode, which is currently under development.

ACKNOWLEDGMENTS

LL is supported by a PhD fellowship from the Region Nouvelle-Aquitaine and the UNIMA engineering consulting company. KM greatly acknowledges the financial support from the University of Bordeaux, through an International Postdoctoral Grant (Idex, nb. 1024R-5030).

LITERATURE CITED

Beetham, E.P. and Kench, P.S., 2011. Field observations of infragravity waves and their behaviour on rock shore platforms. *Earth Surface Processes and Landforms*, 36(14), 1872-1888.

Brayne, R.P., 2015. The relationship between nearshore wave conditions and coarse clastic beach dynamics.

Dodet, G.; Bertin, X.; Bouchette, F.; Gravelle, M.; Testut, L., and Wöppelmann, G., 2019. Characterization of sea-level variations along the metropolitan coasts of France: Waves, tides, storm surges and long-term changes. In press to *Journal of Coastal Research*.

Guérin, T.; Bertin, X.; Coulombier, T., and de Bakker, A., 2018. Impacts of wave-induced circulation in the surf zone on wave setup. *Ocean Modelling*, 123, 86-97.

Guza, R.T.; Thornton, E.B., and Holman, R.A., 1985. Swash on steep and shallow beaches. In *Coastal Engineering 1984* (pp. 708-723).

Falter, J.L.; Atkinson, M.J., and Merrifield, M.A., 2004. Mass-transfer limitation of nutrient uptake by a wave-dominated reef flat community. *Limnology and Oceanography*, 49(5), 1820-1831.

Farrell, E.J.; Granja, H.; Cappietti, L.; Ellis, J.T.; Li, B., and Sherman, D.J., 2009. Wave transformation across a rock platform, Belinho, Portugal. *Journal of Coastal Research*, 44-48.

Jager, T., 2016. Infra-gravity wave transformation across macro-tidal rocky shore platforms.

Longuet-Higgins, M.S. and Stewart, R.W., 1962. Radiation stress and mass transport in gravity waves, with application to 'surf beats'. *Journal of Fluid Mechanics*, 13(4), 481-504.

Lowe, R.J.; Falter, J.L.; Bandet, M.D.; Pawlak, G.; Atkinson, M.J.; Monismith, S.G., and Koseff, J.R., 2005. Spectral wave dissipation over a barrier reef. *Journal of Geophysical Research: Oceans*, 110(C4).

Marshall, R.J. and Stephenson, W.J., 2011. The morphodynamics of shore platforms in a micro-tidal setting: Interactions between waves and morphology. *Marine Geology*, 288(1-4), 18-31.

Naylor, L.A.; Stephenson, W.J., and Trenhaile, A.S., 2010. Rock coast geomorphology: recent advances and future research directions. *Geomorphology*, 114(1-2), 3-11.

Ogawa, H.; Dickson, M.E., and Kench, P.S., 2011. Wave transformation on a sub-horizontal shore platform, Tatapouri, North Island, New Zealand. *Continental Shelf Research*, 31(14), 1409-1419.

Ogawa, H.; Kench, P., and Dickson, M., 2012. Field measurements of wave characteristics on a near-horizontal shore platform, Mahia Peninsula, North Island, New Zealand. *Geographical Research*, 50(2), 179-192.

Ogawa, H., 2013. Observation of wave transformation on a sloping type B shore platform under wind-wave and swell conditions. *Geo-Marine Letters*, 33(1), 1-11.

Ogawa, H.; Dickson, M.E., and Kench, P.S., 2015. Hydrodynamic constraints and storm wave characteristics on a sub-horizontal shore platform. *Earth Surface Processes and Landforms*, 40(1), 65-77.

Poate, T.; Masselink, G.; Austin, M.J.; Dickson, M., and McCall, R., 2018. The role of bed roughness in wave transformation across sloping rock shore platforms. *Journal of Geophysical Research: Earth Surface*, 123(1), 97-123.

Poate, T.; Masselink, G.; Austin, M.J.; Inch, K.; Dickson, M., and McCall, R., 2019. Infragravity wave generation on shore platforms: Bound long wave versus breakpoint forcing. *Geomorphology*, 106880.

Stephenson, W.J. and Kirk, R.M., 2000. Development of shore platforms on Kaikoura Peninsula, South Island, New Zealand: Part one: the role of waves. *Geomorphology*, 32(1-2), 21-41.

Stephenson, W.J.; Naylor, L.A.; Smith, H.; Chen, B., and Brayne, R.P., 2018. Wave transformation across a macrotidal shore platform under low to moderate energy conditions. *Earth Surface Processes and Landforms*, 43(1), 298-311.

Stephenson, W.J.; Kirk, R.M., and Hemmingsen, M.A., 2019. Forty three years of micro-erosion meter monitoring of erosion rates on shore platforms at Kaikōura Peninsula, South Island, New Zealand. *Geomorphology*, 344, 1-9.

Sunamura, T., 1992. *Geomorphology of rocky coasts* (Vol. 3). John Wiley & Son Ltd.

Symonds, G.; Huntley, D.A., and Bowen, A.J., 1982. Two-dimensional surf beat: Long wave generation by a time-varying breakpoint. *Journal of Geophysical Research: Oceans*, 87(C1), 492-498.

Thornton, E.B. and Guza, R.T., 1983. Transformation of wave height distribution. *Journal of Geophysical Research: Oceans*, 88(C10), 5925-5938.

Trenhaile, A.S. and Kanyaya, J.I., 2007. The role of wave erosion on sloping and horizontal shore platforms in macro-and mesotidal environments. *Journal of Coastal Research*, 298-309.

Van Dongeren, A.R.J.A.; Battjes, J.; Janssen, T.; Van Noorloos, J.; Steenhauer, K.; Steenbergen, G., and Reniers, A.J.H.M., 2007. Shoaling and shoreline dissipation of low-frequency waves. *Journal of Geophysical Research: Oceans*, 112(C2).

Zhang, Y.J.; Ye, F.; Stanev, E.V., and Grashorn, S., 2016. Seamless cross-scale modeling with SCHISM. *Ocean Modelling*, 102, 64-81.